Journal of Computational Physics 533 (2025) 113992

Contents lists available at ScienceDirect

Journal of Computational Physics

journal homepage: www.elsevier.com/locate/jcp

A preconditioning method with the *Generalized*−α time discretization for dynamic crack propagations based on XFEM

Xingding Chen [a], Xiao-Chuan Cai [b,*]

[a] School of Mathematics and Statistics, Beijing Technology and Business University, Beijing 100048, PR China
[b] Department of Mathematics, University of Macau, Macau, 999078, PR China

ARTICLE INFO

Keywords:
Dynamic crack propagations
XFEM
Generalized−α methods
Domain decomposition preconditioner

ABSTRACT

In this paper, we consider the efficient simulations of dynamic crack propagations based on the Extended Finite Element Method (XFEM). For the time discretization, the *Generalized*−α method is adopted to instead of the commonly used Newmark method in engineering, and the non physical numerical oscillations can be reduced in the *Generalized*−α method by choosing appropriate parameters. Moreover, in order to accelerate the convergence rate of the linear system arising from XFEM, a special crack-tip domain decomposition preconditioning method is developed, in which the computational domain is decomposed into regular subdomains and crack tip subdomains. To construct the Schwarz preconditioners, the subproblems are solved exactly in the crack tip subdomains and inexactly in the regular subdomains by an incomplete LU factorization. When cracks propagate, only the subdomains around the crack tips are updated, and all the other regular subdomains remain unchanged, which can save the computational cost significantly. The numerical experiments verify that the proposed preconditioning algorithm works well for the simulations of dynamic crack propagations.

1. Introduction

The extended finite element method (XFEM) [1,2] is a powerful numerical technique which is widely used to solve fracture problems with discontinuities, singularities and localized deformations. When simulate crack problems with the standard finite element method (FEM), special meshes are needed whose element edges should be coincide with the crack surfaces and elements nodes should be placed on the crack tips. Moreover, the mesh reconstruction is often needed as cracks propagate, which increase the computational cost significantly. To overcome these difficulties, XFEM introduces some additional enrichment functions to capture the discontinuities along the crack surfaces and the singularities around the crack tips. Then, structured meshes can be adopted to resolve the crack problems, and mesh reconstructions are not required as cracks propagate.

Although XFEM has many advantages, the major drawback is that the linear system arising from XFEM is very ill-conditioned, and robust iterative solvers are needed. Generally, the condition number of the stiffness matrix in XFEM for the linear elastic crack problem is $O(h^{-6})$, while the condition number of the stiffness matrix in FEM is only $O(h^{-2})$, h is the mesh size. One way to reduce the condition number is to modify the enrichment functions, such as the stable generalized finite element methods [3–7] and the improved XFEM [8,9]. In these modified methods, the condition number can be reduced to $O(h^{-2})$ for some cases. The other way

* Corresponding author.
E-mail addresses: chenxd@th.btbu.edu.cn (X. Chen), xccai@um.edu.mo (X.-C. Cai).

https://doi.org/10.1016/j.jcp.2025.113992
Received 19 November 2024; Received in revised form 4 April 2025; Accepted 4 April 2025

Available online 8 April 2025

is the preconditioning techniques, which can reduce the condition number even smaller. There are some works in this category, for example, Luc Berger-Vergiat et al. [10] introduced a multiplicative Schwarz domain decomposition preconditioner for static cracks, which decomposed the physical domain into several cracked subdomains and a healthy subdomain. Waisman et al. [11] adopted this domain decomposition strategy to solve quasi-static crack problems, and two adaptive searching algorithms were needed to update the cracked subdomains. In our previous work, we carefully analysis the small eigenvalues of the stiffness matrix and proposed effective two-level domain decomposition preconditioners for static cracks problems [12]. Moreover, in order to simulate the quasi-static cracks, we constructed a recycling preconditioning method with special initial guesses to accelerate the convergence [13]. For dynamic crack simulations, Svolos et al. [14] proposed a domain decomposition preconditioner based on the phase-field method, which treated all crack regions as a localized subdomain and the remaining part of the computational domain as a healthy subdomain.

The dynamic crack problem considers the crack evolution over time and the corresponding linear system is more complex than the static crack problem as it involves velocity, acceleration and time integration [15,16]. The Newmark method is a popular choice for the time discretization, which includes explicit and implicit schemes. The explicit Newmark scheme [17,18] with a special lumping technique [19,20] is commonly used in the engineering, in which the critical time step size should be small enough to ensure the stability. The implicit Newmark scheme is unconditionally stable and allows a larger time step, but the linear system is highly ill-conditioned, which almost cannot be solved directly by standard linear solvers without any preconditioning. Besides, the construction of the Newmark method is based on the Taylor expansions of smooth functions, if we use the Newmark method for time discretization in dynamic cracks, obvious non physical numerical oscillations in velocity and acceleration are inevitable. So, another time integration scheme could be preferred. Réthoré [21] proposed an implicit integration scheme by incorporating enhancement functions into the time discretization, which is called the time extended finite element method (T-XFEM). T-XFEM has third-order accuracy, allows for larger time steps, and can reduce numerical oscillations to some extent. But the over-damped behavior in T-XFEM causes serious the numerical damping and energy dissipations. As we know, the *Generalized−α* methods [22] with appropriate parameters can be endowed with stability in an energy sense and guarantee energy decay in the high-frequency range as well as asymptotic annihilation. Therefore, in the dynamic cracks simulations, we will choose appropriate *Generalized−α* method for the time discretization to reduce the non physical numerical oscillations, and construct effective domain decomposition preconditioners to solve the linear system arise from the corrected XFEM [23].

This paper is organized as follows. Section 2 describes the general mechanism of the dynamic crack problem, which includes the governing equations, the *Generalized−α* methods for the time discretization and the criteria for the crack propagation. Section 3 presents the domain decomposition preconditioners. In Section 4, the benchmark problem is adopted to test the computational accuracy of different *Generalized−α* methods. Section 5 provides some numerical experiments to investigates the effectiveness of the algorithm. Finally, some concluding remarks are presented in Section 6.

2. XFEM for dynamic crack propagation problems

2.1. The model problem

In this study, we consider an elastic dynamic crack problem. The domain $\Omega \subset \mathcal{R}^2$ with the boundary $\partial\Omega = \Gamma_g \cup \Gamma_u \cup \Gamma_c$. A prescribed displacement $\boldsymbol{u}_0$ and velocity $\dot{\boldsymbol{u}}_0$ are imposed on Γ_u, a boundary force $\boldsymbol{g}$ acts on Γ_g, and the crack surface Γ_c is subject to a constant pressure $\boldsymbol{p}$, as shown in Fig. 1. The initial displacement and velocity in the domain are set to zero. The equilibrium equations and boundary conditions are given as

$$\begin{cases} \nabla \cdot \boldsymbol{\sigma} + \boldsymbol{f} = \rho \ddot{\boldsymbol{u}}, & \text{in } \Omega, \\ \boldsymbol{\sigma} \cdot \boldsymbol{n} = \boldsymbol{g}, & \text{on } \Gamma_g, \\ \boldsymbol{\sigma} \cdot \boldsymbol{n} = \boldsymbol{p}, & \text{on } \Gamma_c, \\ \boldsymbol{u}(\boldsymbol{x}, t) = \boldsymbol{u}_0, & \text{on } \Gamma_u, \\ \dot{\boldsymbol{u}}(\boldsymbol{x}, t) = \dot{\boldsymbol{u}}_0, & \text{on } \Gamma_u, \\ \boldsymbol{u}(\boldsymbol{x}, 0) = 0, & \text{in } \Omega \backslash \Gamma_u, \\ \dot{\boldsymbol{u}}(\boldsymbol{x}, 0) = 0, & \text{in } \Omega \backslash \Gamma_u, \end{cases} \tag{1}$$

where $(\boldsymbol{x}, t)$ is the coordinates and time, ρ is the density, $\dot{\boldsymbol{u}}$ is the velocity, $\ddot{\boldsymbol{u}}$ is the acceleration, $\boldsymbol{f}$ is a given body force acting on the whole domain, and $\boldsymbol{\sigma}$ is the stress tensor corresponding to the displacement $\boldsymbol{u}$.

We assume that the strain and the displacement are small, therefore the kinematical equation consists of the strain-displacement relation is

$$\boldsymbol{\varepsilon} = \boldsymbol{\varepsilon}(\boldsymbol{u}) = \nabla_s \boldsymbol{u},$$

where ∇_s is the symmetric part of the gradient operator, and the constitutive relation is given by the Hooke's law

$$\boldsymbol{\sigma} = \mathbf{C} : \boldsymbol{\varepsilon},$$

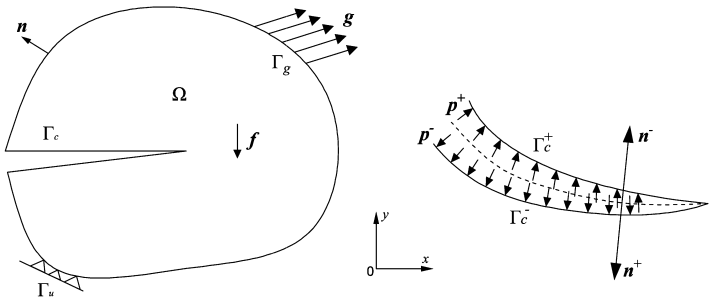

Fig. 1. Diagram of the two-dimensional crack model (the dotted line is the crack line and it is split into two crack surfaces. $\boldsymbol{n}^-$ and $\boldsymbol{n}^+$ are the unit normal vectors to the upper and bottom surfaces of the crack, $\boldsymbol{p}^+$ and $\boldsymbol{p}^-$ are the crack pressure above and below the crack line, respectively).

where **C** is the Hooke tensor.

The solution of (1) lies in the space of admissible displacement

$$\boldsymbol{U} = \{\boldsymbol{u} \,|\, \boldsymbol{u} \in [\boldsymbol{H}^1(\Omega \backslash \Gamma_c)]^2, \boldsymbol{u} = \boldsymbol{u}_0 \text{ on } \Gamma_u,\ \boldsymbol{u} \text{ is discontinuous across } \Gamma_c\}, \tag{2}$$

where $\boldsymbol{H}^1(*)$ is the standard Sobolev space related to the regularity of the solution. A detailed description for the domain with an internal boundary can be found in [24]. We note that the space $\boldsymbol{H}^1(*)$ allows for discontinuous functions across the crack line. The test function space is defined similarly as

$$\boldsymbol{V} = \{\boldsymbol{v} \,|\, \boldsymbol{v} \in [\boldsymbol{H}_0^1(\Omega \backslash \Gamma_c)]^2, \boldsymbol{v} = 0 \text{ on } \Gamma_u,\ \boldsymbol{v} \text{ is discontinuous across } \Gamma_c\}. \tag{3}$$

The weak form of the governing equation (1) is to find $\boldsymbol{u} \in \boldsymbol{U}$ such that

$$\int_\Omega \rho \ddot{\boldsymbol{u}} \cdot \boldsymbol{v} d\Omega + \int_\Omega \varepsilon(\boldsymbol{u}) : C : \varepsilon(\boldsymbol{v}) d\Omega = \int_\Omega \boldsymbol{f} \cdot \boldsymbol{v} d\Omega + \int_{\Gamma_g} \boldsymbol{g} \cdot \boldsymbol{v} d\Gamma + \int_{\Gamma_c} \boldsymbol{p} \cdot \boldsymbol{v} d\Gamma, \quad \forall \boldsymbol{v} \in \boldsymbol{V}. \tag{4}$$

It is shown in Belytschko and Black [1] that the above weak form is equivalent to the strong form (1), including the traction condition on the crack line.

To discretize (4), the corrected XFEM [23] is applied, which uses level set functions to detect the locations of the nodes around the crack and its tips, and a ramp function to handle the blending area. There are two types of typical enrichment functions to enrich the nodes along cracks, see [1,2].

Heaviside enrichment function: all the nodes along the crack, excluding those at the tips, are enriched by the Heaviside function to incorporate a strong discontinuity

$$H(\boldsymbol{x}) = \begin{cases} +1 & \text{if } (\boldsymbol{x} - \boldsymbol{x}_c) \cdot \boldsymbol{n}_c^- \geq 0, \\ -1 & \text{otherwise}, \end{cases} \tag{5}$$

where $\boldsymbol{n}_c^-$ is the unit normal vector to the negative side of the crack surface, and $\boldsymbol{x}_c$ is a point on the crack surface that has the shortest distance to $\boldsymbol{x}$.

Branch enrichment functions: nodes of the elements containing or near crack tips are enriched with a set of four functions, that model the near-tip analytical solution by incorporating the tip singularities, i.e., for $\alpha = 1, \cdots, 4$,

$$\phi^\alpha(r(\boldsymbol{x}), \theta(\boldsymbol{x})) = \left\{ \sqrt{r} sin\left(\frac{\theta}{2}\right), \sqrt{r} cos\left(\frac{\theta}{2}\right), \sqrt{r} sin\left(\frac{\theta}{2}\right) sin\theta, \sqrt{r} cos\left(\frac{\theta}{2}\right) sin\theta \right\}, \tag{6}$$

where $(r(\boldsymbol{x}), \theta(\boldsymbol{x}))$ is a polar coordinate system centered at the crack tip $\boldsymbol{x}$. In this local polar coordinate system, the crack tip $\boldsymbol{x}$ is typically chosen as the origin. Here $r(\boldsymbol{x})$ denotes the radial distance measured from the crack tip to a mesh point, and $\theta(\boldsymbol{x})$ signifies the angular value between the position of that mesh point and the direction in which the crack propagates.

Then, the general expression of the corrected XFEM solution of the Equation (4) can be written as

$$\boldsymbol{u}_h(\boldsymbol{x}) = \sum_{i \in N_S} \varphi_i(\boldsymbol{x}) \boldsymbol{u}_i + \sum_{j \in N_H} \varphi_j(\boldsymbol{x}) \left[H(\boldsymbol{x}) - H\left(\boldsymbol{x}_j\right)\right] \boldsymbol{a}_j + \sum_{k \in N_{tip}} \sum_{\alpha=1}^{4} \varphi_k(\boldsymbol{x}) \left[\phi^\alpha(\boldsymbol{x}) - \phi^\alpha\left(\boldsymbol{x}_k\right)\right] \mathcal{R}(\boldsymbol{x}) \boldsymbol{b}_k^\alpha, \tag{7}$$

where N_S, N_H, and N_{tip} represent the set of all mesh points, the nodal subset from elements cut by cracks, and the nodal subset from elements around the crack tips within an enrichment radius r_{tip}, respectively. φ_i, φ_j, and φ_k are the standard FEM shape functions. $\boldsymbol{u}_i$ is the unknowns associated with the nodal set N_s. $\boldsymbol{a}_j$ and $\boldsymbol{b}_\alpha^k$ are the unknowns for the enriched nodal subset N_H and N_{tip}. $\mathcal{R}(x)$ represents a ramp function employed to overcome the problem of blending elements [25]. The enrichment strategy is illustrated in Fig. 2.

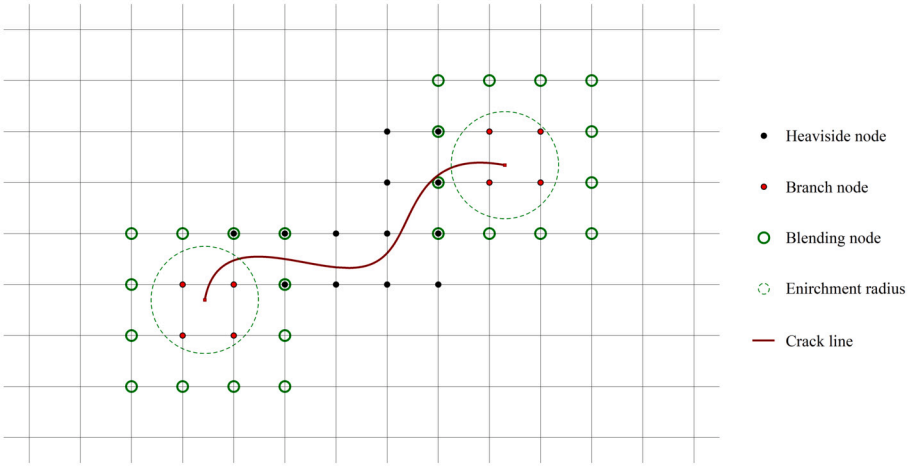

Fig. 2. The enrichment scheme for the corrected XFEM on a structured mesh. The red curve represents the crack, the black dots are points enriched by the Heaviside function, the red dots are points enriched by branch enrichment functions, the little green circles denote the nodes from blending elements, and the dotted green circles are the area where the branch enrichments are applied. (For interpretation of the colors in the figure(s), the reader is referred to the web version of this article.)

Replace the infinite displacement $\boldsymbol{u}$ by the finite approximation $\boldsymbol{u}_h(\boldsymbol{x})$ in the weak form (4), we have

$$\mathbb{M}\ddot{\mathbf{U}} + \mathbb{K}\mathbf{U} = \mathbf{F}, \tag{8}$$

where $\mathbb{M}$ is the mass matrix, $\mathbb{K}$ is the stiffness matrix, $\mathbf{F}$ is the force vector, $\ddot{\mathbf{U}}$ is the nodal acceleration vector $\ddot{\mathbf{U}} = \left[\ddot{\boldsymbol{u}}_i, \ddot{\boldsymbol{a}}_j, \ddot{\boldsymbol{b}}_k^{\alpha}\right]$, and $\mathbf{U}$ is the displacement vector $\mathbf{U} = \left[\boldsymbol{u}_i, \boldsymbol{a}_j, \boldsymbol{b}_k^{\alpha}\right]$. The corresponding discretized formulae are

$$\begin{cases} (\mathbb{M})_{ij} = \displaystyle\int_{\Omega} \rho\bar{\varphi}_i\bar{\varphi}_j d\Omega, \\ (\mathbb{K})_{ij} = \displaystyle\int_{\Omega} \nabla_s^{\mathrm{T}}\bar{\varphi}_i\mathbf{C}\nabla_s^{\mathrm{T}}\bar{\varphi}_j d\Omega, \\ (\mathbf{F})_i = \displaystyle\int_{\Gamma_c} p\bar{\varphi}_i d\Gamma + \int_{\Gamma_g} g\bar{\varphi}_i d\Gamma + \int_{\Omega} f\bar{\varphi}_i d\Omega, \end{cases} \tag{9}$$

where $\bar{\varphi}_i$ can be chosen as $\varphi_i, \varphi_i H(\boldsymbol{x})$ or $\varphi_i\phi^{\alpha}(\boldsymbol{x})$ according to the different type of the nodes, and the value of $\bar{\varphi}_j$ is similar.

2.2. The Generalized−α method

In engineering, the Newmark method [26] is commonly used for the time discretization, which can be represented as an explicit/implicit method by choosing different parameters. However, the construction of the Newmark method is based on the Taylor expansions of smooth functions, which can not handle discontinuous problems very well. If we use the Newmark integrators in dynamic fracture mechanics, both the velocity and the acceleration exhibit obvious numerical oscillations, see details in [21]. So, another time integration scheme could be preferred.

In this study, the *Generalized−α* method [22] is adopted for the time discretization. Assume that the displacement vector $\mathbf{U}$ and the velocity vector $\dot{\mathbf{U}}$ are continuous functions at the time t, then we can get the *Generalized−α* method by introducing two new parameters α_m, α_f in the Newmark method, namely

$$\mathbb{M}\ddot{\mathbf{U}}_{n+1-\alpha_m} + \mathbb{K}\mathbf{U}_{n+1-\alpha_f} = \mathbf{F}_{n+1-\alpha_f}, \tag{10a}$$

$$\mathbf{U}_{n+1} = \mathbf{U}_n + \Delta t\dot{\mathbf{U}}_n + \Delta t^2((\frac{1}{2} - \beta)\ddot{\mathbf{U}}_n + \beta\ddot{\mathbf{U}}_{n+1}), \tag{10b}$$

$$\dot{\mathbf{U}}_{n+1} = \dot{\mathbf{U}}_n + \Delta t((1-\gamma)\ddot{\mathbf{U}}_n + \gamma\ddot{\mathbf{U}}_{n+1}), \tag{10c}$$

where

$$\mathbf{U}_{n+1-\alpha_f} = (1-\alpha_f)\mathbf{U}_{n+1} + \alpha_f\mathbf{U}_n, \quad \dot{\mathbf{U}}_{n+1-\alpha_f} = (1-\alpha_f)\dot{\mathbf{U}}_{n+1} + \alpha_f\dot{\mathbf{U}}_n,$$
$$\ddot{\mathbf{U}}_{n+1-\alpha_m} = (1-\alpha_m)\ddot{\mathbf{U}}_{n+1} + \alpha_m\ddot{\mathbf{U}}_n, \quad \mathbf{F}_{n+1-\alpha_f} = (1-\alpha_f)\mathbf{F}_{n+1} + \alpha_f\mathbf{F}_n.$$

For the *Generalized−α* method, the displacement vector $\mathbf{U}_{n+1}$ and acceleration vector $\ddot{\mathbf{U}}_{n+1}$ should be computed implicitly. Substitute equation (10b) into equation (10a) and solve a linear system with unknowns $\ddot{\mathbf{U}}_{n+1}$ to get the acceleration. After that, we get

Table 1
Relations among the algorithmic parameters in order to achieve first order accuracy for the Newmark method, second-order accuracy for the α-methods and corresponding unconditional stability conditions.

Method	α_m	α_f	β	γ
Newmark	0	0	$\frac{1}{4}(\gamma+\frac{1}{2})^2$	$\geqslant \frac{1}{2}$
HHT$-\alpha$	0	$0 \leqslant -\alpha_{HHT} \leqslant \frac{1}{2}$	$\frac{1}{4}(1-\alpha_{HHT})^2$	$\frac{1}{2}-\alpha_{HHT}$
WBZ$-\alpha$	$\alpha_{WBZ} \leqslant 0$	0	$\frac{1}{4}(1-\alpha_{WBZ})^2$	$\frac{1}{2}-\alpha_{WBZ}$
CH$-\alpha$	$3\alpha_f - 1$	$\leqslant \frac{1}{2}$	$(1-\alpha_f)^2$	$\frac{3}{2}-2\alpha_f$

Table 2
Relations among the algorithmic parameters of the Newmark method and the α-methods expressed as functions of the spectral radius ρ_∞ and corresponding ranges, where $\beta = \frac{1}{(1+\rho_\infty)^2}, \gamma = \frac{1}{2}\frac{3-\rho_\infty}{1+\rho_\infty}$ for all the methods.

Method	ρ_∞	α_m	α_f
Newmark	$-\frac{2\gamma-3}{1+2\gamma} \in [0,1]$	0	0
HHT$-\alpha$	$\frac{1+\alpha_{HHT}}{1-\alpha_{HHT}} \in [\frac{1}{2},1]$	0	$-\alpha_{HHT} = \frac{1-\rho_\infty}{1+\rho_\infty} \in [0,\frac{1}{3}]$
WBZ$-\alpha$	$\frac{1+\alpha_{WBZ}}{1-\alpha_{WBZ}} \in [0,1]$	$\alpha_{WBZ} = \frac{\rho_\infty-1}{1+\rho_\infty} \in [-1,0]$	0
CH$-\alpha$	$\frac{\alpha_f}{1-\alpha_f} \in [0,1]$	$\frac{2\rho_\infty-1}{1+\rho_\infty} \in [-1,\frac{1}{2}]$	$\frac{\rho_\infty}{1+\rho_\infty} \in [0,\frac{1}{2}]$

back to equation (10b) to compute the displacement $\mathbf{U}_{n+1}$, and finally go to equation (10c) to compute the velocity $\dot{\mathbf{U}}_{n+1}$. The linear system solved by the single-step *Generalized*$-\alpha$ method can be written as

$$\begin{aligned}[\mathbb{M}(1-\alpha_m)+(1-\alpha_f)\beta\Delta t^2\mathbb{K}]\mathbf{U}_{n+1} &= [\mathbb{M}(1-\alpha_m)-\alpha_f\beta\Delta t^2\mathbb{K}]\dot{\mathbf{U}}_n \\ &+ \mathbb{M}(1-\alpha_m)\Delta t\dot{\mathbf{U}}_n + \frac{1}{2}\mathbb{M}(1-\alpha_m-2\beta)\Delta t^2\ddot{\mathbf{U}}_n + \beta\Delta t^2\mathbf{F}_{n+1-\alpha_f},\end{aligned} \tag{11}$$

where $\mathbf{U}_n, \dot{\mathbf{U}}_n, \ddot{\mathbf{U}}_n$ are the displacement, velocity and acceleration vectors at the nth time step, respectively, which are known for the current time step $n+1$.

After get $\mathbf{U}_{n+1}$, $\ddot{\mathbf{U}}_{n+1}$ and $\dot{\mathbf{U}}_{n+1}$ can be calculated by equations (10b)-(10c), namely

$$\ddot{\mathbf{U}}_{n+1} = \frac{\mathbf{U}_{n+1} - (\mathbf{U}_n + \Delta t\dot{\mathbf{U}}_n + (\frac{1}{2}-\beta)\Delta t^2\ddot{\mathbf{U}}_n)}{\beta\Delta t^2}, \tag{12}$$

$$\dot{\mathbf{U}}_{n+1} = \dot{\mathbf{U}}_n + (1-\gamma)\Delta t\ddot{\mathbf{U}}_n + \gamma\Delta t\ddot{\mathbf{U}}_{n+1}. \tag{13}$$

In equation (10b), the displacement at the time step $n+1$ is calculated from the displacement, velocity and acceleration at the time step n. As the crack propagates, the enrichments at the time step n and $n+1$ are different, that is the number of DOFs at the time step $n+1$ is usually larger than that of the time step n. To make the formula (10b) computable, the solutions $(\mathbf{U}_n, \dot{\mathbf{U}}_n, \ddot{\mathbf{U}}_n)$ at the time step n should be extended to the size of the time step $n+1$.

To avoid accumulate too many DOFs in the linear system (11) when the crack propagates, we use the enrichment strategy in [27]. Suppose that, from time step t_n to t_{n+1}, the crack tip propagates from one element to another element, the crack tip area at the time step t_n will become an area across the crack line, which is only enriched by the Heaviside function.

Therefore, for the evolution from t_n to t_{n+1}, the solutions of the branch enrichment DOFs at t_n are discarded, the solutions of the overlapping Heaviside DOFs and regular DOFs are preserved, and the initial values for the newly introduced Heaviside DOFs and branch enrichment DOFs are set to zero. To sum up, the solutions from t_n to t_{n+1} have the following formulation

$$[\mathbf{U}_n]^{(n+1)} = \left[[\mathbf{U}_n]^{(n)}_{reg},\ [\mathbf{U}_n]^{(n)}_{hvi},\ [\mathbf{O}]^{(n+1)}_{hvi},\ [\mathbf{O}]^{(n+1)}_{tip} \right]^T, \tag{14}$$

where $[\mathbf{U}_n]^{(n)}_{reg}$, $[\mathbf{U}_n]^{(n)}_{hvi}$ refer to the regular DOFs and the Heaviside DOFs at t_n. $[\mathbf{O}]^{(n+1)}_{hvi}$ and $[\mathbf{O}]^{(n+1)}_{tip}$ are zero vectors, related to the newly introduced Heaviside DOFs and branch enrichment DOFs at t_{n+1}, respectively.

2.3. The parameters in the Generalized$-\alpha$ method

In principle, the parameters $\alpha_m, \alpha_f, \beta, \gamma$ in the *Generalized*$-\alpha$ method are independent of each other. However, in order to guarantee the compatibility, stability and favorable dissipation in the formula (11), the relationships between these parameters are established and three typical *Generalized*$-\alpha$ methods can be achieved, which are shown in Table 1-Table 3, see the details in [22].

Considering the relations among the algorithmic parameters from Table 1-Table 3, we can give the parameters in the *Generalized*$-\alpha$ methods, namely

Table 3
Unconditional stability conditions for the algorithmic parameters of the *Generalized−α* method, where S denotes Stability, O.D. denotes Optimal Dissipation and S.O.A. denotes Second Order Accuracy.

Parameter conditions	α_m	α_f	β	γ
S	$\frac{1}{2}-(\gamma-\alpha_f)\leqslant\alpha_m\leqslant\frac{1}{2}$	$\leqslant\frac{1}{2}$	$\geqslant\frac{\gamma}{2}$	$\geqslant\frac{1}{2}$
S and O.D. (99)	$\frac{1}{2}-(\gamma-\alpha_f)\leqslant\alpha_m\leqslant\frac{1}{2}$	$\leqslant\frac{1}{2}$	$\frac{1}{4}(\gamma+\frac{1}{2})^2$	$\geqslant\frac{1}{2}$
S and S.O.A. (101)	$\leqslant\alpha_f$	$\leqslant\frac{1}{2}$	$\geqslant\frac{1}{4}+\frac{1}{2}(\alpha_f-\alpha_m)$	$\frac{1}{2}+\alpha_f+\alpha_m$
S, (99) and (101)	$\leqslant\alpha_f$	$\leqslant\frac{1}{2}$	$\frac{1}{4}(1+\alpha_f-\alpha_m)^2$	$\frac{1}{2}+\alpha_f+\alpha_m$

CH−α method:

$$\alpha_m=\alpha_f=\frac{1}{2},\beta=\frac{1}{4},\gamma=\frac{1}{2},\text{then }\rho_\infty=1, \tag{15}$$

HHT−α method:

$$\alpha_m=0,\alpha_f=\frac{1}{3},\beta=\frac{4}{9},\gamma=\frac{5}{6},\text{then }\rho_\infty=0.5, \tag{16}$$

WBZ−α method:

$$\alpha_m=-1,\alpha_f=0,\beta=1,\gamma=\frac{3}{2},\text{then }\rho_\infty=0. \tag{17}$$

where $\rho_\infty=\rho(\Omega),\Omega\to\infty$ is the spectral radius at infinity, $\rho_\infty\in[0,1]$. The choice $\rho_\infty=0$ corresponds to the case of asymptotic annihilation of the high-frequency response, while $\rho_\infty=1$ corresponds to the case of no algorithmic dissipation. Note that, when we choose $\alpha_m=\alpha_f=0$ in the CH−α method, it degenerates into an implicit Newmark method. In section 4, we will test the performance of the above *Generalized−α* methods by a benchmark problem.

2.4. The dynamic crack propagations

In dynamic fracture mechanics, the crack propagation is usually determined by the following steps, and each step may be obtained with different techniques or criterions. In this paper we choose the popular methods.

- Step 1: Computation of the dynamic stress intensity factors, e.g., by the J-integral method [28].
  We utilize a variant of the J-integral method, known as the interaction integral, to extract the mixed-mode DSIFs (Dynamic Stress Intensity Factors). The interaction integral $I^{(1,2)}$ is defined as

$$\begin{aligned}I^{(1,2)}=&-\int_A q_{k,j}\left[\left(\sigma_{ml}^{aux}u_{m,l}-\rho\dot{u}_l\dot{u}_l^{aux}\right)\delta_{kj}-\left(\sigma_{ij}^{aux}u_{i,k}+\sigma_{ij}u_{i,k}^{aux}\right)\right]\mathrm{d}A\\&+\int_A q_k\left[\left(\sigma_{ij,j}^{aux}u_{i,k}+\ddot{u}_iu_{i,k}^{aux}\right)+\left(\rho\dot{u}_i^{aux}\dot{u}_{i,k}+\rho\dot{u}_i\dot{u}_{i,k}^{aux}\right)\right]\mathrm{d}A\\&-\int_{S^+\!+S^-}t_ju_{j,1}^{aux}q\,dS,\end{aligned} \tag{18}$$

  where the auxiliary fields include the auxiliary displacement field u_i^{aux}, the auxiliary stress field σ_{ij}^{aux}, the auxiliary velocity field $\dot{u}_i^{aux}$, and their spatial derivatives, see [29] for the details. The relationship between the interaction integral $I^{(1,2)}$ and DSIFs is

$$I^{(1,2)}=\frac{2}{E^*}\left(f_1(\dot{a})K_{\mathrm{I}}^{dyn}K_{\mathrm{I}}^{aux}+f_2(\dot{a})K_{\mathrm{II}}^{dyn}K_{\mathrm{II}}^{aux}\right), \tag{19}$$

  where K_{I}^{dyn} and K_{II}^{dyn} are the actual dynamic mode-I and mode-II DSIFs, respectively, K_{I}^{aux} and K_{II}^{aux} are the auxiliary SIFs. $f_1(\dot{a})$ and $f_2(\dot{a})$ are two universal functions which are related to the crack velocity $\dot{a}$ and material parameters,

$$\begin{cases}f_1(\dot{a})=\dfrac{4\alpha_d\left(1-\alpha_s^2\right)}{(\kappa+1)D},\ f_2(\dot{a})=\dfrac{4\alpha_s\left(1-\alpha_s^2\right)}{(\kappa+1)D},\\[2ex]\alpha_{\mathrm{d}}=\sqrt{1-\left(\dfrac{\dot{a}}{c_{\mathrm{d}}}\right)^2},\ \alpha_{\mathrm{s}}=\sqrt{1-\left(\dfrac{\dot{a}}{c_{\mathrm{s}}}\right)^2},\\[2ex]c_{\mathrm{d}}=\sqrt{\dfrac{\lambda+2\mu}{\rho}},\ c_{\mathrm{s}}=\sqrt{\dfrac{\mu}{\rho}},\\[2ex]D=4\alpha_{\mathrm{d}}\alpha_{\mathrm{s}}-\left(1+\alpha_{\mathrm{s}}^2\right)^2,\end{cases} \tag{20}$$

where c_d and c_s are the dilatational and shear wave speeds, respectively [30]. The material constants are determined by the following equations for plane stress

$$E^* = E,\ \lambda = \frac{E\nu}{1-\nu^2},\ \mu = \frac{E}{2(1+\nu)},\ \kappa = \frac{3-\nu}{1+\nu}.$$

where E is the Young's modules, ν is the Poisson's ratio.

By assuming the different state of the auxiliary field, the actual dynamic SIFs can be obtained separately in the following way,

$$\begin{cases} K_{\mathrm{I}}^{dyn} = \dfrac{E^*}{2f_1(\dot{a})} I^{(1,2)}, \text{ when } K_{\mathrm{I}}^{aux} = 1, \text{ and } K_{\mathrm{II}}^{aux} = 0, \\ K_{\mathrm{II}}^{dyn} = \dfrac{E^*}{2f_2(\dot{a})} I^{(1,2)}, \text{ when } K_{\mathrm{I}}^{aux} = 0, \text{ and } K_{\mathrm{II}}^{aux} = 1. \end{cases} \tag{21}$$

- Step 2: Verification of the crack stability (whether the crack will propagate or not), determined by the fracture toughness or fracture energy criterions, based on the maximum circumferential (hoop) stress criterion.

  The stability criteria are written as

$$\begin{cases} K_{\theta\theta}^{dyn} < K_{IC}, & \text{crack is stable (will not propagate)}, \\ K_{\theta\theta}^{dyn} \geqslant K_{IC}, & \text{crack is unstable (will propagate)}, \end{cases}$$

  where K_{IC} is the fracture toughness, and $K_{\theta\theta}^{dyn}$ is the equivalent stress intensity factor, and can be expressed by

$$K_{\theta\theta}^{dyn} = \cos^3\left(\frac{\theta_c}{2}\right) K_{\mathrm{I}}^{dyn} - \frac{3}{2}\cos\left(\frac{\theta_c}{2}\right)\sin\left(\theta_c\right) K_{\mathrm{II}}^{dyn}, \tag{22}$$

  the crack's direction θ_c is given by

$$\theta_c = 2\arctan\left[\frac{1}{4}\left(\frac{K_{\mathrm{I}}^{dyn}}{K_{\mathrm{II}}^{dyn}} - \mathrm{sign}\left(K_{\mathrm{II}}^{dyn}\right)\sqrt{8+\left(\frac{K_{\mathrm{I}}^{dyn}}{K_{\mathrm{II}}^{dyn}}\right)^2}\right)\right], \tag{23}$$

  where the "sign" is a signal function.
- Step 3: Compute the velocity of the crack propagation.

  The speed of the crack tip propagation $\dot{a}$ is obtained by

$$\dot{a} = \begin{cases} 0, & K_{\theta\theta}^{dyn} < K_{IC}, \\ c_r\left(1 - \dfrac{K_{IC}}{K_{\theta\theta}^{dyn}}\right)^{\frac{1}{m}}, & K_{\theta\theta}^{dyn} \geq K_{IC}, \end{cases} \tag{24}$$

  where c_r is the Rayleigh wave velocity [31], m is an arbitrary parameter used to get better agreement with experimental data. m can be set as $m = 1$, $m = 2$ or other numbers according to prior knowledge, see [17,32] for details.

3. The domain decomposition preconditioners

Because of the singularity of the asymptotic field around the crack tip, the linear system (11) is difficult to solve using the classical iterative methods [33]. In order to accelerate the convergence, the preconditioning techniques are required. One of the popular preconditioning methods is the domain decomposition method (DDM), which partitions the global problem into some sub-problems and solve these sub-problems independently to construct a preconditioner for the global problem.

To apply DDM for the linear systems (11), it is important to choose a suitable strategy to decompose the degrees of freedom into subsets. In [10], the domain is partitioned into cracked subdomains and a healthy subdomain, in which each crack is involved in a cracked subdomain. When cracks propagate, not only extra subdomain updating strategies are needed, but also the scales of cracked subdomains become larger and larger, which increases the computational cost obviously [34]. In this paper, we give a new domain decomposition strategy, which can separate the DOFs of the branch enrichment functions from the remaining DOFs, and do not need any extra searching algorithms to update the subdomains when the cracks propagate.

3.1. The crack-tip domain decomposition

As discovered in [35], the tip enhancement has a huge impact on the eigenvalue distribution of the stiffness matrix near zero, and the small eigenvalues of the stiffness matrix are all associated with the crack tips, then we can propose a special "crack-tip" domain decomposition.

The computational domain is divided into two types of subdomains: the regular subdomains Ω^{reg} and the crack-tip subdomains Ω^{tip}, see Fig. 3. The crack-tip subdomains include all the branch enriched nodes, which have strong impact on the convergence of

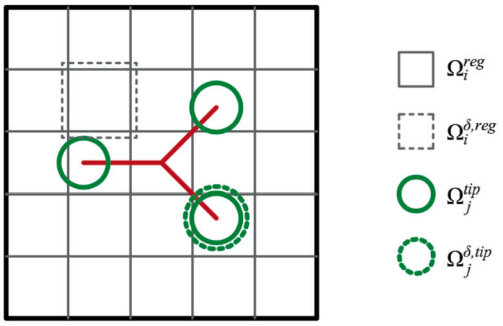

Fig. 3. The "crack-tip" domain decomposition.

the iterative methods; the regular subdomains include the Heaviside enriched nodes and can pass through cracks, which have very little influence on the convergence rate of the iterative methods. Note that $\Omega^{reg} \cap \Omega^{tip} = \emptyset$. Extend all the subdomains with δ lays of the nodes from the neighboring subdomains to form the overlapping subdomains $\Omega^{\delta,reg}$ and $\Omega^{\delta,tip}$, then

$$\Omega = \sum_{i=1}^{n_{reg}} \Omega_i^{reg} \cup \sum_{j=1}^{n_{tip}} \Omega_j^{tip} = \sum_{i=1}^{n_{reg}} \Omega_i^{\delta,reg} \cup \sum_{j=1}^{n_{tip}} \Omega_j^{\delta,tip},$$

where the n_{reg}, n_{tip} are the number of regular subdomains and crack-tip subdomains, respectively. The regular subdomains Ω^{reg} and $\Omega^{\delta,reg}$ only include the regular DOFs and Heaviside DOFs, and the crack tip subdomains Ω^{tip} and $\Omega^{\delta,tip}$ include the regular DOFs, the Heaviside DOFs and the branch enrichment DOFs.

3.2. Additive and restricted additive Schwarz preconditioners

Based on the "crack-tip" domain decomposition, we present additive Schwarz (AS) and restricted additive Schwarz (RAS) preconditioners for the Krylov subspace method GMRES [36] to solve the sequence of linear systems (11).

We first define the subdomain restriction matrix $\mathbb{R}_i^{\delta}$ which is a sub-identity matrix whose diagonal entries are one or zero, and $\mathbb{R}_i^{\delta}\mathbf{U}$ keeps the components of $\mathbf{U}$ in Ω_i^{δ} unchanged, and zeros at all other components. The regular subdomain stiffness matrix $\mathbb{M}_i$ ($\mathbb{M}_i = \widetilde{\mathbb{M}}|_{\Omega_i^{\delta}},\ i = 1, \cdots, n_{reg}$) and the crack-tip subdomain stiffness matrix $\mathbb{M}_j$ ($\mathbb{M}_j = \widetilde{\mathbb{M}}|_{\Omega_j^{\delta}},\ j = 1, \cdots, n_{tip}$) are defined as follows:

$$\mathbb{M}_i = (\mathbb{R}_i^{\delta})^T \widetilde{\mathbb{M}} \mathbb{R}_i^{\delta}, \quad \mathbb{M}_j = (\mathbb{R}_j^{\delta})^T \widetilde{\mathbb{M}} \mathbb{R}_j^{\delta},$$

Where $\widetilde{\mathbb{M}} = \mathbb{M}(1-\alpha_m) + (1-\alpha_f)\beta\Delta t^2 \mathbb{K}$ is the coefficient matrix in equation (11). The AS and RAS preconditioned methods are described in Algorithm 1 and Algorithm 2, respectively, see [37,38] for details.

Remark 1. In Algorithm 1 and Algorithm 2, incomplete LU factorization (ILU) is utilized to construct the preconditioner for regular subproblems. Since the regular subdomains Ω^{reg} do not contain branch enhanced nodes, any inexact solvers can be applied to solve these regular subproblems. As a result, commonly-used techniques, such as incomplete Cholesky factorization and the algebraic multigrid method, can be employed as inexact solvers. For example, the authors in [10] made use of the algebraic multigrid method to construct a multiplicative Schwarz domain decomposition preconditioner for static crack problems.

Remark 2. It is important to note that there exist multiple approaches to applying a preconditioner to a linear system, including left preconditioning, right preconditioning, and double-sided preconditioning. Given that the right-preconditioned residual is equivalent to the residual of the original unpreconditioned problem, we have chosen to employ the right-preconditioned GMRES method in this paper. For more in-depth information regarding the preconditioning technique, readers can refer to Chapter 9 of [36].

Algorithm 1 Additive Schwarz preconditioned Krylov subspace method.

Solve a sequence of systems of varying sizes

$$\widetilde{\mathbb{M}}\mathbb{M}_{\mathrm{AS}}^{-1}\mathbf{U}^* = \widetilde{\mathbf{F}},\ \mathbf{U}^* = \mathbb{M}_{\mathrm{AS}}\mathbf{U}$$

by a Krylov subspace method, where $\widetilde{\mathbf{F}}$ is the right-hand term of (11) and the preconditioner is defined by

$$\mathbb{M}_{\mathrm{AS}}^{-1} = \sum_{i=1}^{n_{reg}} (R_i^{\delta})^T \mathbb{M}_i^{-1} R_i^{\delta} + \sum_{j=1}^{n_{tip}} (R_j^{\delta})^T \mathbb{M}_j^{-1} R_j^{\delta},$$

where $(\mathbb{M}_i)^{-1} (i = 1, \cdots, n_{reg})$ is a subspace inverse of $\widetilde{\mathbb{M}}$ and is solved inexactly as usual (such as ILU), but the subdomain systems corresponding to $\mathbb{M}_j (j = 1, \cdots, n_{tip})$ are solved exactly.

Algorithm 2 Restricted additive Schwarz preconditioned Krylov subspace method.

Solve a sequence of systems of varying sizes

$$\widetilde{\mathbb{M}}\mathbb{M}_{\mathrm{RAS}}^{-1}\mathbf{U}^{*}=\widetilde{\mathbf{F}},\ \mathbf{U}^{*}=\mathbb{M}_{\mathrm{RAS}}\mathbf{U}$$

by a Krylov subspace method, where $\widetilde{\mathbf{F}}$ is the right-hand term of (11) and the preconditioner is defined by

$$\mathbb{M}_{\mathrm{RAS}}^{-1}=\sum_{i=1}^{n_{reg}}(R_i^0)^T\mathbb{M}_i^{-1}R_i^{\delta}+\sum_{j=1}^{n_{tip}}(R_j^0)^T\mathbb{M}_j^{-1}R_j^{\delta},$$

where $(\mathbb{M}_i)^{-1}(i=1,\cdots,n_{reg})$ is a subspace inverse of $\widetilde{\mathbb{M}}$ and is solved inexactly as usual (such as ILU), but the subdomain systems corresponding to $\mathbb{M}_j(j=1,\cdots,n_{tip})$ are solved exactly, $\mathbb{R}_i^0$ is defined similar as $\mathbb{R}_i^{\delta}$, which is from the global domain Ω to the local non-overlapping subdomain Ω_i.

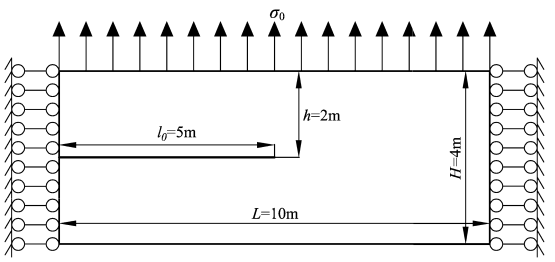

Fig. 4. The geometry and boundary conditions for the benchmark crack model (L, H are the length and height of the plate, h is the distance from the crack line to the top edge, l_0 is the crack length, and σ_0 is a boundary loading).

4. Verification

In this section, we develop a MATLAB code based on the corrected XFEM to study the computational performance of different *Generalized*−α methods in Section 2.3. In order to ensure the correctness and accuracy of the code, a benchmark problem is adopted to verify the calculation of dynamic SIFs as it is crucial for the propagation of a moving crack.

Considering an infinite plate with a semi-infinite crack as shown in Fig. 4, the left and right edges are fixed on the x-direction. A uniform tensile traction $\sigma_0 = 500MPa$ is applied on the top edge. The plate size is $10m\times 4m$, and the initial crack with length $l_0 = 5m$ is located at the left center of the plate. The material parameters are, the Young's modules $E = 210GPa$, the Poisson's ratio $\upsilon = 0.30$, and the density $\rho = 8000Kg/m^3$.

Assume the crack propagation velocity $\dot{a}(t)$ is

$$\dot{a}=\begin{cases}0 & \text{if } t<m\cdot t_c,\\ 1500 & \text{if } t\geq m\cdot t_c,\end{cases} \tag{25}$$

then the analytical solution of the mode I dynamic SIFs for this problem is available in [39] has the form

$$K_1(\dot{a},t)=\begin{cases}0 & \text{if } t<t_c,\\ \dfrac{2\sigma_0}{1-\nu}\sqrt{\dfrac{c_1(t-t_c)(1-2\nu)}{\pi}} & \text{if } t_c\leq t<1.5t_c,\\ \dfrac{2\sigma_0}{1-\nu}\sqrt{\dfrac{c_1(t-t_c)(1-2\nu)}{\pi}}\gamma(\dot{a}) & \text{if } 1.5t_c\leq t,\end{cases} \tag{26}$$

where $t_c = h/c_d$ is the time that the stress wave first reaches the crack tip, c_d is the velocity of the dilatational wave, h is the mesh size, and $\gamma(\dot{a})$ is

$$\gamma(\dot{a})=\frac{1-\dfrac{\dot{a}}{c_r}}{1-\dfrac{\dot{a}}{2c_r}}. \tag{27}$$

In this calculation, we set $t_c = 3.36\times 10^{-4}s, c_1 = 5944m/s, c_r = 2947m/s$, the time step $\Delta t = 5\times 10^{-5}s$, and the mesh scale is 50×50. The total number of time steps is set to 20, that the total simulation time is $1ms$. We take different values of m in (25), then calculate the model I dynamic SIFs and the crack tip propagation velocity using different *Generalized*−α methods, see (15)-(17). In the Newmark method, we set $\beta=\frac{1}{2},\gamma=\frac{1}{4}$, which can obtain an implicit scheme.

- **Test 1**: choose $m = 1$, the crack starts propagating when $t > t_c$ with a constant velocity $\dot{a} = 1500m/s$.

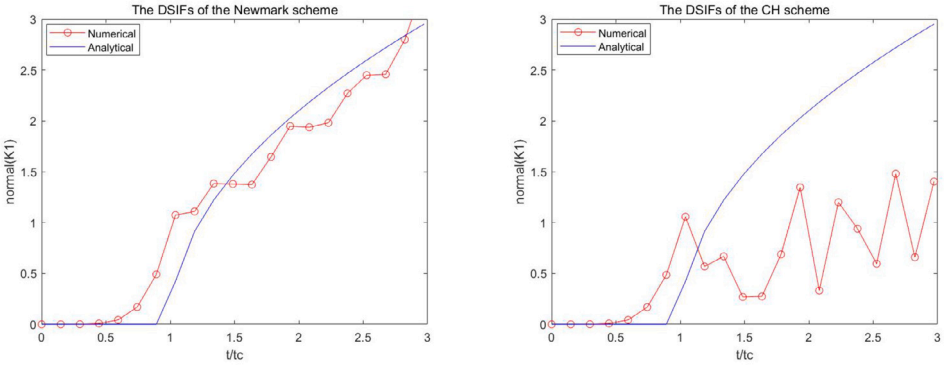

(a) K_I of the Newmark scheme

(b) K_I of the CH$-\alpha$ scheme

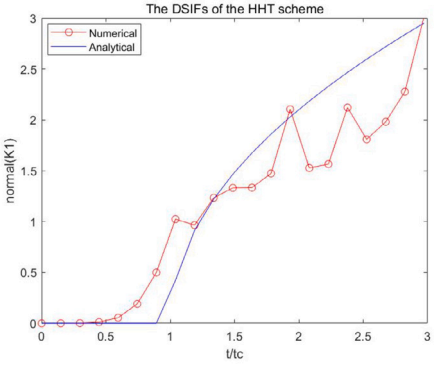

(c) K_I of the HHT$-\alpha$ scheme

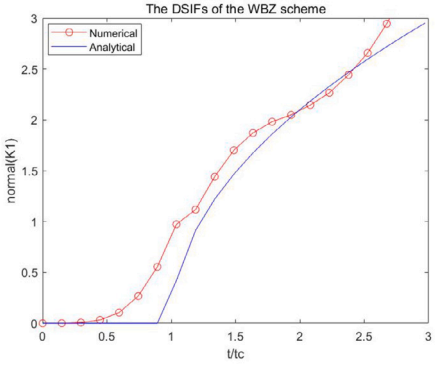

(d) K_I of the WBZ$-\alpha$ scheme

Fig. 5. The model I dynamic stress intensity factors K_I obtained by different time discretizations in test 1, normal ($K1$) denotes $K1/(\sigma_0 h^{0.5})$.

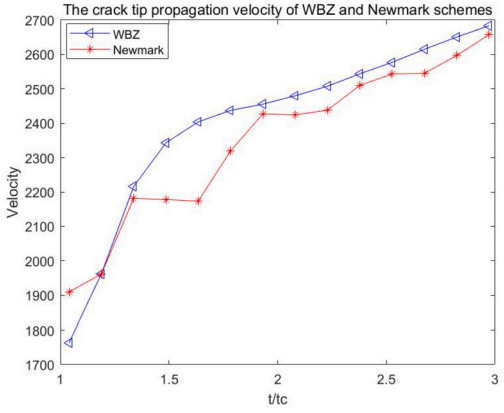

Fig. 6. The crack tip propagation velocity in test 1.

Fig. 5 shows the numerical DSIFs calculated by different time discretizations. We can see that the numerical DSIFs of the CH$-\alpha$ method and the HHT$-\alpha$ method differ significantly from the analytical DSIF, while the numerical results of the Newmark method and the WBZ$-\alpha$ method can match well with the analytical DSIF. Moreover, from Fig. 5(a) and 5(d), we clearly see that there exist obvious numerical oscillations in the Newmark method, but the DSIF curve in the WBZ$-\alpha$ method is much more smooth, which means that the WBZ$-\alpha$ method can reduce the numerical oscillations effectively.

Fig. 6 shows the crack tip propagation velocity calculated by the Newmark method and the WBZ$-\alpha$ method. It can be seen that the velocity curve of the WBZ$-\alpha$ method varies smoothly over time, while the velocity in the Newmark method has significant numerical oscillations.

- **Test 2**: choose $m = 1.5$, the crack starts propagating when $t > 1.5t_c$ with a constant velocity $\dot{a} = 1500m/s$.

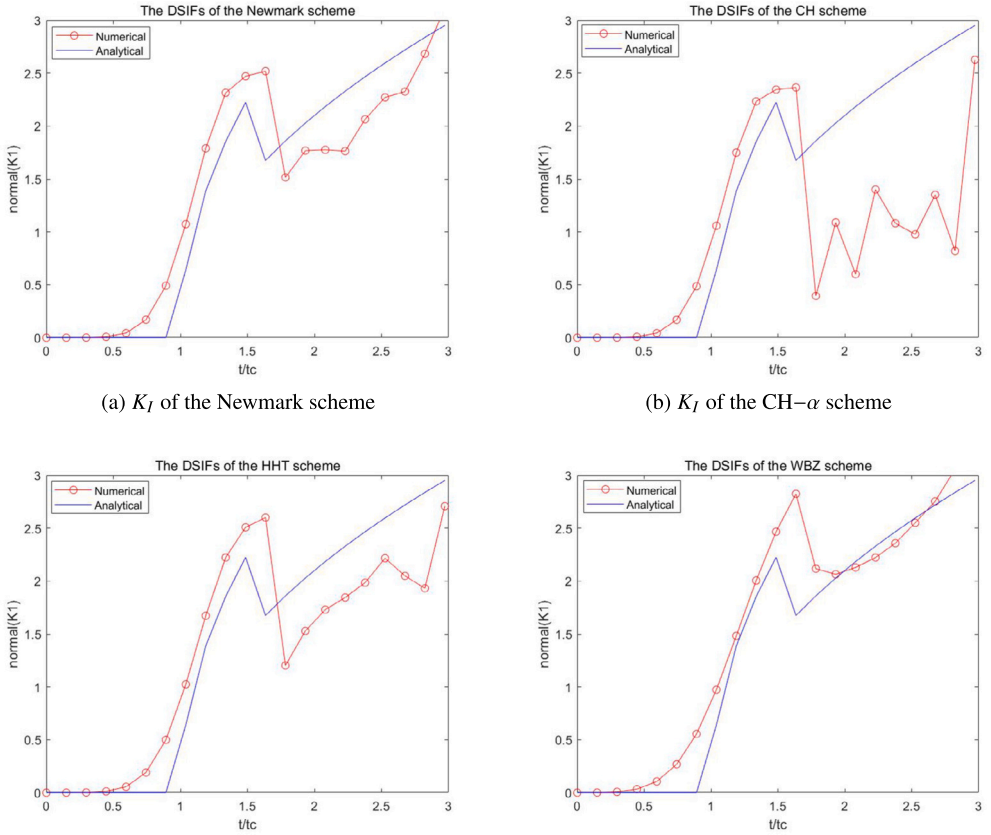

(a) K_I of the Newmark scheme

(b) K_I of the CH$-\alpha$ scheme

(c) K_I of the HHT$-\alpha$ scheme

(d) K_I of the WBZ$-\alpha$ scheme

Fig. 7. The model I stress intensity factors K_I obtained by the different time discretizations in test 2, normal(K1) denotes $K1/(\sigma_0 h^{0.5})$.

From Fig. 7, we can see that the numerical DSIFs calculated by the Newmark method and the WBZ$-\alpha$ method match better with the analytical DSIF than the other two methods. Comparing Fig. 7(a) and Fig. 7(d), it is clear that the WBZ$-\alpha$ method can reduce the numerical oscillations obviously.

Fig. 8 gives the numerical solutions of the crack propagation velocity in the Newmark method and the WBZ$-\alpha$ method. We can see that the WBZ$-\alpha$ method can still reduce the numerical oscillations obviously in this test.

- **Test 3**: choose $m = 1$, use different mesh scales and time steps in the Newmark method and the WBZ$-\alpha$ method.

It is shown in test 1 and test 2 that the Newmark method and the WBZ$-\alpha$ method perform better than the other $Generalized-\alpha$ methods, so we only compare these two methods under different mesh scales and time steps. First, we fix the time step $\Delta t = 5e-5s$, the mesh scale varies from $50\times 50, 100\times 100$ to 200×200. The numerical solutions of the dynamic stress intensity factors and crack tip propagation velocity are shown in Fig. 9 and Fig. 10, respectively. From these figures, we can see that the numerical solutions obtained by the Newmark method still exhibit numerical oscillations as mesh refinements, while the WBZ$-\alpha$ method can reduce the numerical oscillations obviously.

Then, we fix the mesh scale 50×50, and the time step is reduced to $\Delta t = 2.5e-5s$. The numerical solutions of the dynamic stress intensity factors and crack tip propagation velocity are shown in Fig. 11 and Fig. 12, respectively. From these figures, we can see that the numerical solutions obtained by the Newmark method exhibits significate oscillations when the time step decreases, but the WBZ$-\alpha$ method can reduce the numerical oscillations and are more consistent with the actual situations.

From test 1 to test 3, we can clearly see that the WBZ$-\alpha$ method can obviously reduce the numerical oscillations both in the calculations of DSIFs and the crack tip propagation velocity.

Remark 3. Regarding the performance of various Generalized$-\alpha$ methods, Hilber and Hughes [40] conducted an investigation into the overshooting effect of the HHT$-\alpha$ method through asymptotic analysis. In their work [41], Hilbert and Hughes demonstrated that the HHT$-\alpha$ scheme is prone to velocity overshoot, and the accuracy of the acceleration calculation in this scheme is only of first order. Subsequently, it has also been proven that the CH$-\alpha$ method retains these undesirable characteristics. For more comprehensive and detailed discussions about the Generalized$-\alpha$ method, interested readers can refer to the content presented in [22].

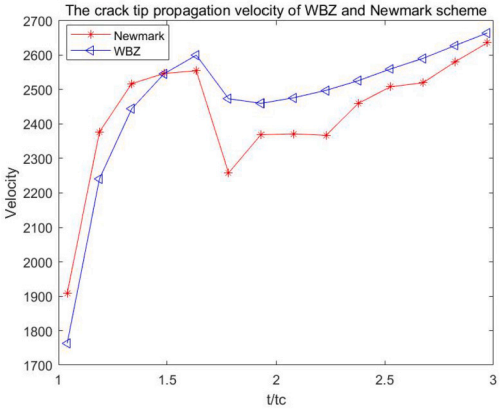

Fig. 8. The crack tip propagation velocity in test 2.

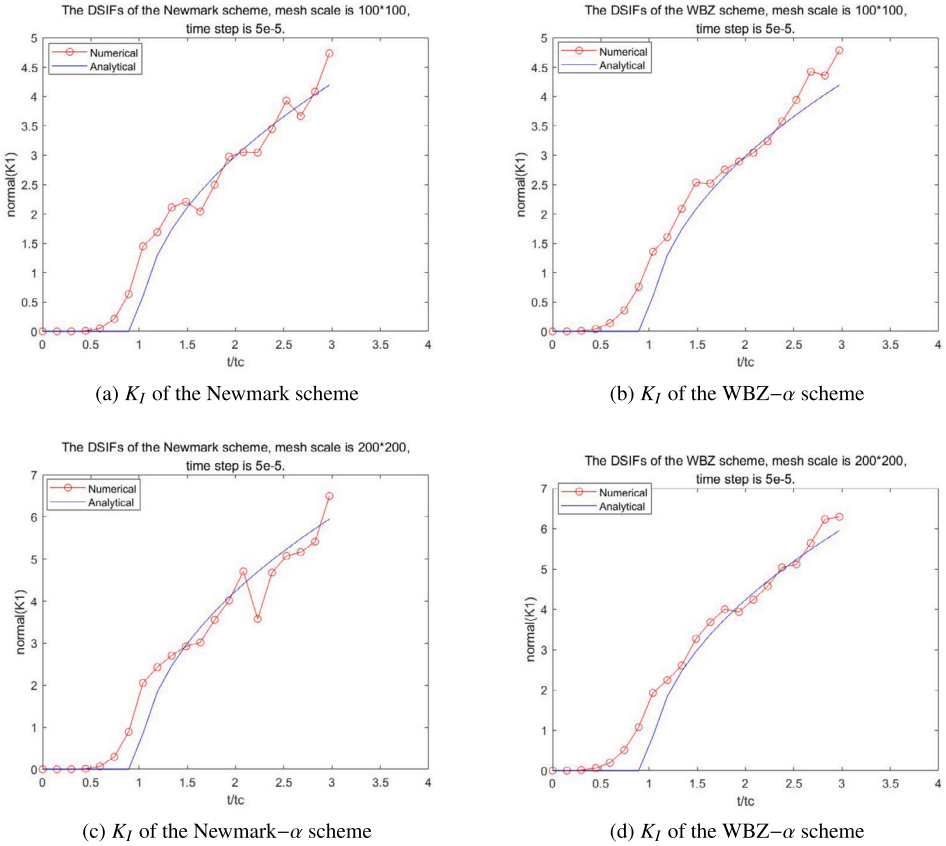

(a) K_I of the Newmark scheme

(b) K_I of the WBZ−α scheme

(c) K_I of the Newmark−α scheme

(d) K_I of the WBZ−α scheme

Fig. 9. The model I stress intensity factors K_I obtained under different mesh scales in test 3, normal(K1) denotes $K1/(\sigma_0 h^{0.5})$.

5. Numerical experiments

In this section, we test the effect of the additive Schwarz and restricted additive Schwarz preconditioners by the benchmark problem shown in Fig. 4. Moreover, the computational accuracy of multiple dynamic cracks propagations using different time discretizations is discussed.

5.1. The performance of the preconditioners

The parameters of the infinite plate with a semi-infinite crack model are the same as in Section 4. We set $m = 1$ in the crack velocity $\dot{a}(t)$, which means the crack starts propagating when $t > t_c$ with a constant velocity $\dot{a} = 1500m/s$. In Section 4, we compared the

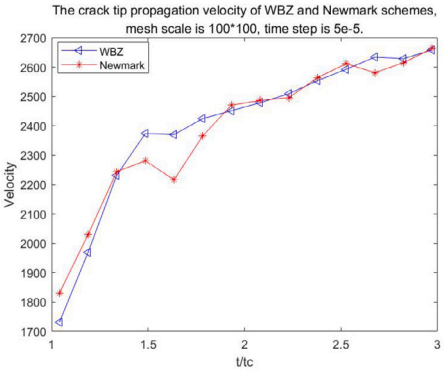

(a) The crack tip velocity, the mesh scale is $100 * 100$

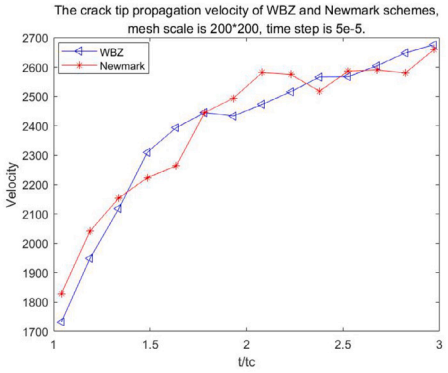

(b) The crack tip velocity, the mesh scale is $200 * 200$

Fig. 10. The crack tip propagation velocity under different mesh scales in test 3.

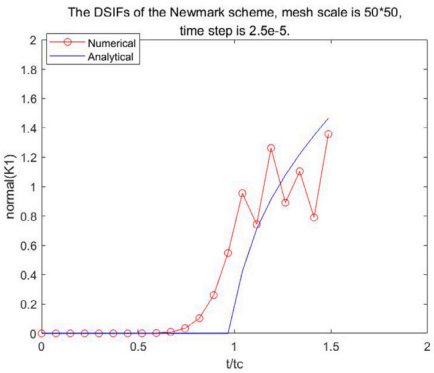

(a) K_I of the Newmark scheme

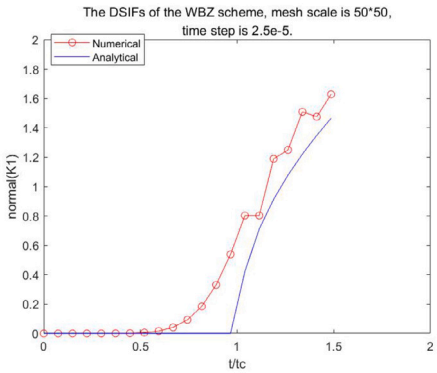

(b) K_I of the WBZ$-\alpha$ scheme

Fig. 11. The model I stress intensity factors K_I when $\Delta t = 2.5e-5s$ in test 3, normal(K1) denotes $K1/(\sigma_0 h^{0.5})$.

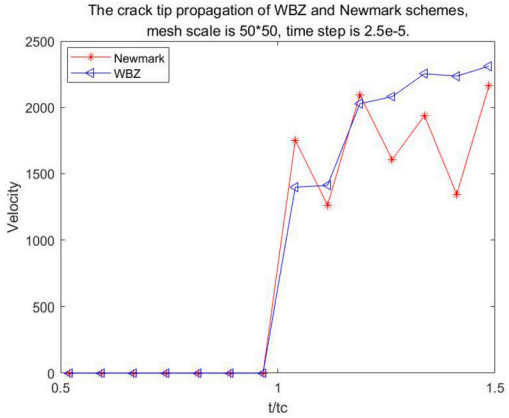

Fig. 12. The crack tip propagation velocity when $\Delta t = 2.5e-5s$ in test 3.

performance of the Newmark method and the *Generalized*$-\alpha$ methods, and the WBZ$-\alpha$ method can reduce the numerical oscillations obviously. So, we will adopt the WBZ$-\alpha$ method for the time discretization.

The parameters in the WBZ$-\alpha$ method are set to $\alpha_m = -1, \alpha_f = 0, \beta = 1, \gamma = \frac{3}{2}$ and $\Delta t = 0.01s$. The computational domain is divided into $m * m$ regular subdomains, then the total number of subdomains is $m * m + 1$. In the AS/RAS preconditioners, we use direct solvers in the "crack-tip" subdomain, and inexact solvers such as ILU in the regular subdomains. The overlapping size is $\delta = 2$, and the ILU drop tolerance for the regular subdomain solver is 10^{-3}. The GMRES method is used as the linear solver and the stopping condition and restart number of GMRES are set 10^{-6} and 100, respectively.

Table 4
The number of iterations at different time steps using the AS preconditioner, nStep denotes the time step, the number of the regular subdomains is $m * m$, and the mesh scale is $n \times n$.

nStep	$4 * 4$		$6 * 6$		$8 * 8$	
	50×50	70×70	50×50	70×70	50×50	70×70
0	15	17	16	18	16	18
1	15	18	17	18	17	19
2	16	18	17	19	17	19
3	16	19	17	19	17	19
4	17	19	18	19	17	19
5	17	19	18	20	17	20
6	17	19	18	20	17	20
7	17	19	18	20	17	20
8	17	18	17	19	17	19

Table 5
The number of iterations at different time steps using the RAS preconditioner, nStep denotes the time step, the number of the regular subdomains is $m * m$, and the mesh scale is $n \times n$.

nStep	$4 * 4$		$6 * 6$		$8 * 8$	
	50×50	70×70	50×50	70×70	50×50	70×70
0	14	15	14	15	14	16
1	14	16	15	16	15	16
2	15	17	16	16	15	17
3	15	17	16	17	15	17
4	15	17	16	16	15	18
5	15	17	16	17	15	18
6	15	17	16	17	15	18
7	15	17	16	17	15	17
8	15	16	15	16	15	17

Table 6
The number of iterations at different time steps using different drop tolerance in ILU, nStep denotes the time step, dpl denotes drop tolerance, the number of the regular subdomains is $6 * 6$, and the mesh scale is 50×50.

nStep	AS		RAS	
	$drt = 10^{-1}$	$drt = 10^{-5}$	$drt = 10^{-1}$	$drt = 10^{-5}$
0	23	12	21	11
1	25	13	22	12
2	26	14	22	13
3	26	15	24	13
4	27	15	25	13
5	27	15	25	13
6	27	15	25	13
7	27	15	25	13
8	27	15	26	12

From Table 4 and Table 5, we can see that the AS/RAS preconditioners can significantly accelerate the convergence rates. When we fix the mesh scale and increase the number of subdomains, the number of iterations in both the AS and RAS preconditioning algorithms are stable, which is very hard to achieve in one-level Schwarz preconditioning methods, but we have achieved this good characteristic by adopting the WBZ$-\alpha$ time discretization method. When we fix the number of subdomains and refine the mesh, the number of iteration increase very slightly. In addition, the RAS preconditioner needs fewer iterations to converge than the AS preconditioner.

It should be noted that when the drop tolerance of the ILU solvers within the regular subdomains is altered, the influence on the computational efficiency can be seen in Table 6. As is evident, with the gradual decrease of the drop tolerance, the number of iterations of the AS/RAS preconditioners also gradually diminishes. When the drop tolerance is lower than 10^{-3}, the number of iterations does not change substantially. Thus, it suffices to adopt the value of 10^{-3} in ILU.

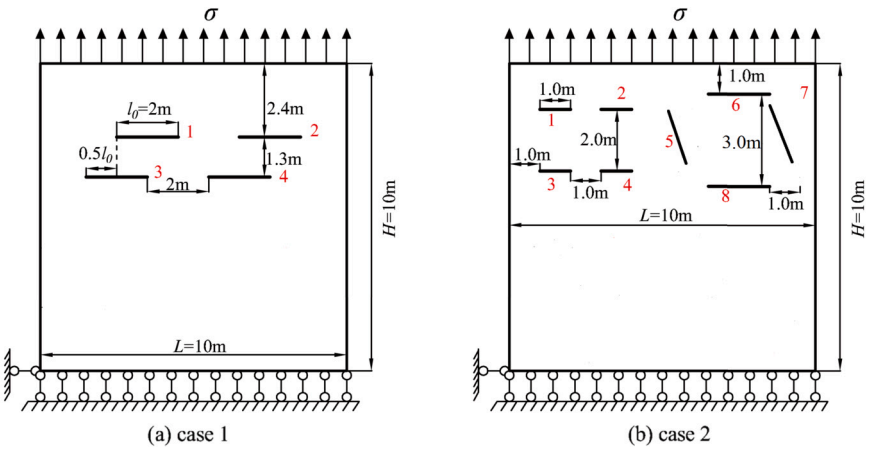

Fig. 13. The multiple cracks models.

Table 7
The number of iterations at different time steps for case 1 and case 2 using the RAS preconditioner, nStep denotes the time step, the number of the regular subdomains is $6 * 6$ or $8 * 8$, and the mesh scale is 150×150.

nStep	$6 * 6$		$8 * 8$	
	case 1	case 2	case 1	case 2
0	8	7	8	8
1	8	8	9	8
2	9	9	9	10
3	9	10	9	10
4	9	10	9	11
5	9	11	9	11
6	9	11	9	12
7	10	13	9	12
8	10	13	10	12

5.2. Multiple cracks simulations

In this section, some complicated multiple cracks cases are used to study the performance of the proposed algorithms. As shown in Fig. 13, a square domain of size $10m \times 10m$ with some pre-existing cracks inside is considered. In this simulation, the Young's modulus $E = 210GPa$, the Poisson's ratio $\nu = 0.30$, the density of solid $\rho = 8000Kg/m^3$, and the critical stress intensity factor $K_{IC} = 0.5MPa$. In Fig. 13(a), the 4 pre-existing cracks are parallel with an initial crack length $l_0 = 2.0m$ and the overlapping length is $0.5l_0$. The bottom edge is fixed in the y-direction and the bottom-left point is fixed in all directions. A uniform tensile traction $\sigma = 10.0MPa$ is applied on the top edge. In Fig. 13(b), 8 pre-existing cracks are located in the domain. The fixed boundary conditions and boundary force are the same as that in Fig. 13(a).

The problem type for both cases is plain stress. The labels of the crack are denoted by the red number. The linear discretized system is solved by the GMRES method with the RAS preconditioner proposed in previous sections. The GMRES parameters are set as follows: the relative convergence tolerance is 10^{-6}, the restart number is 50, the ILU drop tolerance for the subdomain solver is 10^{-3}. The mesh size is 150×150 and the time step is set as $\Delta t = 10^{-4}s$. The total time steps is 50, which means the total simulated physical time is $5ms$. The crack propagation velocity $\dot{a}$ is computed by (24).

We use the Newmark method and the WBZ$-\alpha$ method for the time discretization, respectively. The numerical solutions of the mode I DSIFs of different cracks in case1 and case2 are shown in Fig. 14 and Fig. 15, respectively. From these figures, we can see that the DSIFs calculated by the Newmark method exhibit significant numerical oscillations, while the DSIFs calculated by the WBZ$-\alpha$ method are relatively smooth and much more reasonable. Therefore, we adopt the WBZ$-\alpha$ method for the time discretization. The number of iterations at different time steps for case 1 and case 2 is shown in Table 7, and the multiple cracks propagations and the Von-Misses stress are plotted in Fig. 16.

6. Conclusions

In engineering, the Newmark method is commonly used for the time discretization. But if we use the Newmark method to discrete the dynamic cracks, there exist significant non physical numerical oscillations in the simulations. In order to reduce the numerical

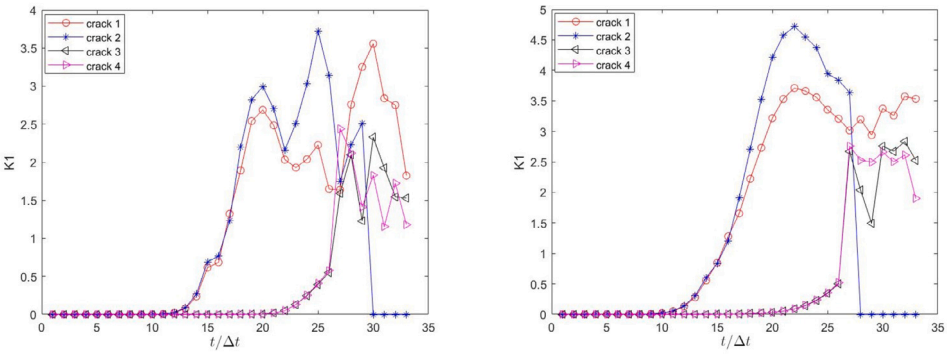

(a) K_I of the Newmark scheme (b) K_I of the WBZ−α scheme

Fig. 14. The DSIFs of the cracks in case 1 by using different time discretizations.

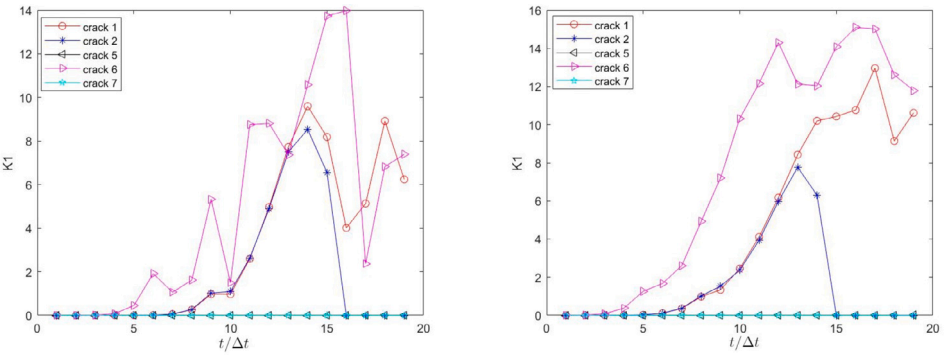

(a) K_I of the Newmark scheme (b) K_I of the WBZ−α scheme

Fig. 15. The DSIFs of the cracks in case 2 by using different time discretizations.

oscillations, the *Generalized*−α time discretization methods combined with the corrected XFEM are adopted to solve the elastic dynamic crack problems in this paper.

The relations of the parameters in the *Generalized*−α methods are established to ensure the second-order accuracy, stability and optimal dissipations. Moreover, we choose appropriate parameters in different *Generalized*−α methods to reduce the non physical numerical oscillations. The benchmark problem shows that the WBZ−α method, can not only reduce non physical numerical oscillations obviously, but also the achieved numerical DSIFs are much more consistent with the analytical DSIFs during crack propagations.

Beside, in order to accelerate the GMRES solver for the algebraic system, the AS/RAS preconditioners are constructed based on a special crack-tip domain decomposition. In these preconditioners, the crack-tip subproblems are solved directly, and the regular subproblems are solved inexactly by ILU. The numerical experiments show that the corresponding preconditioners can significantly accelerate the convergence arte, and the number of iterations are stable as the mesh refined or the number of subdomains increased.

CRediT authorship contribution statement

Xingding Chen: Writing – review & editing, Writing – original draft, Software, Conceptualization. **Xiao-Chuan Cai:** Writing – review & editing, Supervision, Methodology.

Declaration of competing interest

We declare that we have no financial and personal relationships with other people or organizations that can inappropriately influence our work, there is no professional or other personal interest of any nature or kind in any product, service and/or company that could be construed as influencing the position presented in, or the review of, the manuscript entitled.

Acknowledgements

The authors are supported by the Disciplinary funding of Beijing Technology and Business University, Natural Science Foundation of China 12071469, FDCT 0141/2020/A3, 0079/2021/AFJ; MYRG-GRG 2023-00102-FST-UMDF.

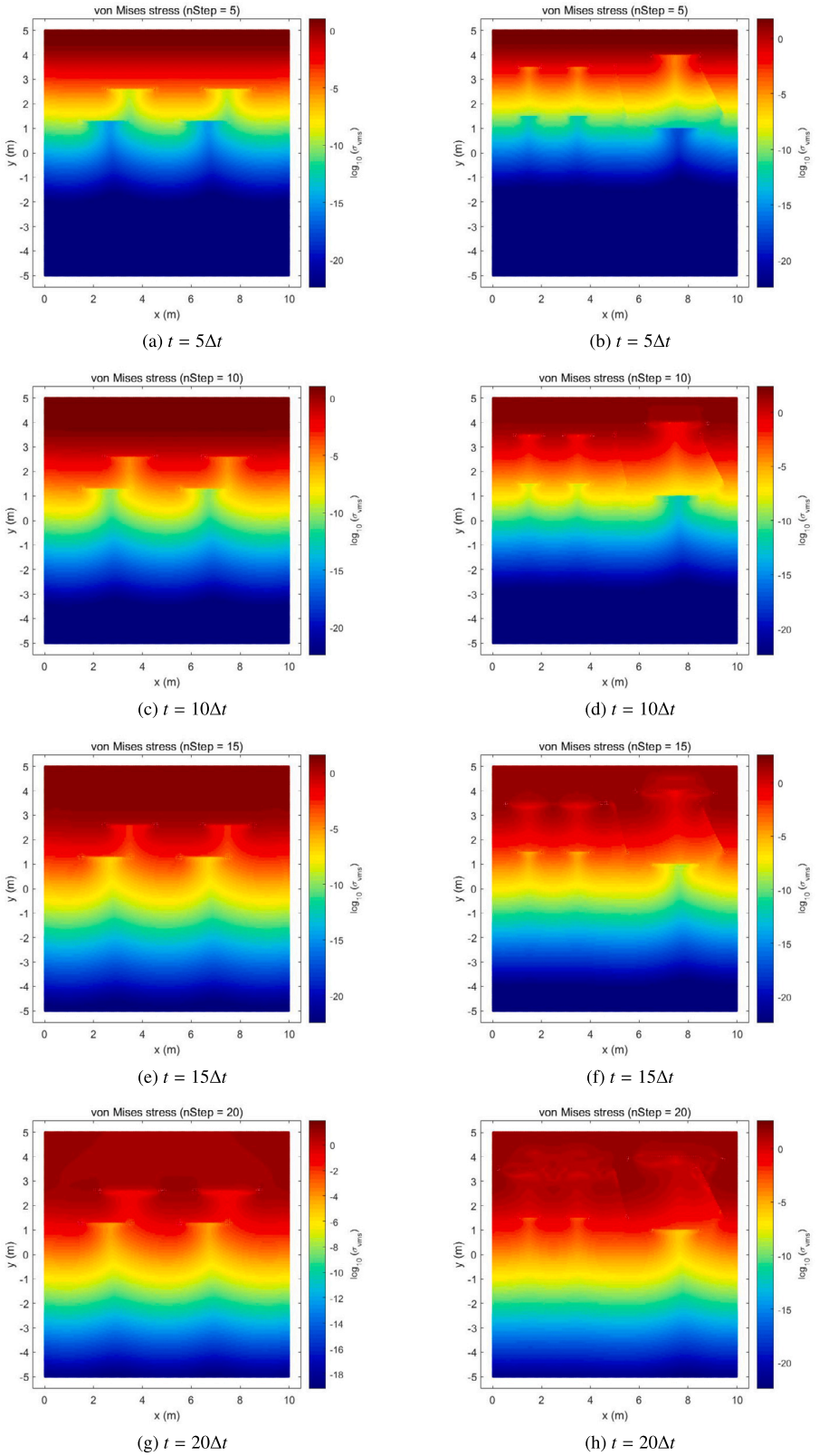

(a) $t = 5\Delta t$ (b) $t = 5\Delta t$

(c) $t = 10\Delta t$ (d) $t = 10\Delta t$

(e) $t = 15\Delta t$ (f) $t = 15\Delta t$

(g) $t = 20\Delta t$ (h) $t = 20\Delta t$

Fig. 16. The Von-Misses stress contour for the multiple moving cracks problem, Δt is the time step, the left figures are for case 1, and the right figures are for case 2.

Data availability

No data was used for the research described in the article.

References

[1] T. Belytschko, T. Howard Black, Elastic crack growth in finite elements with minimal remeshing, Int. J. Numer. Methods Eng. 45 (1999) 601–620.
[2] N. Mose, J. Dolbow, T. Belytschko, A finite element method for crack growth without remeshing, Int. J. Numer. Methods Eng. 46 (1999) 131–150.
[3] I. Babuška, U. Banerjee, Stable generalized finite element method (sgfem), Comput. Methods Appl. Mech. Eng. 201 (2012) 91–111.
[4] I. Babuška, U. Banerjee, K. Kergrene, Strongly stable generalized finite element method: application to interface problems, Comput. Methods Appl. Mech. Eng. 327 (2017) 58–92.
[5] V. Gupta, C. Duarte, I. Babuška, U. Banerjee, A stable and optimally convergent generalized fem (sgfem) for linear elastic fracture mechanics, Comput. Methods Appl. Mech. Eng. 266 (2013) 23–39.
[6] Q. Zhang, I. Babuška, U. Banerjee, Robustness in stable generalized finite element methods (sgfem) applied to Poisson problems with crack singularities, Comput. Methods Appl. Mech. Eng. 311 (2016) 476–502.
[7] Q. Zhang, I. Babuška, A stable generalized finite element method (sgfem) of degree two for interface problems, Comput. Methods Appl. Mech. Eng. 363 (2020) 112889.
[8] R. Tian, L. Wen, L. Wang, Three-dimensional improved xfem (ixfem) for static crack problems, Comput. Methods Appl. Mech. Eng. 343 (2019) 339–367.
[9] L. Wang, L. Wen, J. Wang, R. Tian, Implementations of parallel software for crack analyses based on the improved xfem, Comput. Methods Appl. Mech. Eng. 48 (2018) 1241–1258.
[10] L. Berger-Vergiat, H. Waisman, B. Hiriyur, R. Tuminaro, D. Keyes, Inexact Schwarz-algebraic multigrid preconditioners for crack problems modeled by extended finite element methods, Int. J. Numer. Methods Eng. 90 (2012) 311–328.
[11] H. Waisman, L. Berger-Vergiat, An adaptive domain decomposition preconditioner for crack propagation problems modeled by XFEM, Int. J. Multiscale Comput. Eng. 11 (2013) 633–654.
[12] X. Chen, X.-C. Cai, An effective Schwarz preconditioner for crack problems modeled by extended finite element method, Commun. Comput. Phys. 28 (2020) 1561–1584.
[13] X. Chen, X.-C. Cai, A recycling preconditioning method with auxiliary tip subspace for elastic crack propagation simulation using XFEM, J. Comput. Phys. 452 (2022) 110910.
[14] L. Svolos, L. Berger-Vergiat, H. Waisman, Updating strategy of a domain decomposition preconditioner for parallel solution of dynamic fracture problems, J. Comput. Phys. 422 (2020) 109746.
[15] S. Kumar, I. Singh, B. Mishra, A. Singh, New enrichments in XFEM to model dynamic crack response of 2-D elastic solids, Int. J. Impact Eng. 87 (2016) 198–211.
[16] J. Réthoré, A. Gravouil, A. Combescure, An energy-conserving scheme for dynamic crack growth using the extended finite element method, Int. J. Numer. Methods Eng. 63 (2005) 631–659.
[17] T. Menouillard Julien, Julien, A. Combescure, H. Bung, Efficient explicit time stepping for the eXtended Finite Element Method (XFEM), Int. J. Numer. Methods Eng. 68 (2006) 911–939.
[18] A. Gravouil, T. Elguedj, H. Maigre, An explicit dynamics extended finite element method. Part 2: element-by-element stable-explicit/explicit dynamic scheme, Comput. Methods Appl. Mech. Eng. 198 (2009) 2318–2328.
[19] T. Menouillard, J. Réthoré, N. Moes, A. Combescure, H. Bung, Mass lumping strategies for X-FEM explicit dynamics: application to crack propagation, Int. J. Numer. Methods Eng. 74 (2008) 447–474.
[20] P. Rozycki, N. Moës, E. Bechet, C. Dubois, X-FEM explicit dynamics for constant strain elements to alleviate mesh constraints on internal or external boundaries, Comput. Methods Appl. Mech. Eng. 197 (2008) 349–363.
[21] N. Mose, J. Dolbow, T. Belytschko, A combined space-time extended finite element method, Int. J. Numer. Methods Eng. 64 (2005) 260–284.
[22] S. Erlicher, L. Bonaventura, O. Bursi, The analysis of the generalized-α method for non-linear dynamic problems, Comput. Mech. 28 (2002) 83–104.
[23] T.-P. Fries, A corrected XFEM approximation without problems in blending elements, Int. J. Numer. Methods Eng. 75 (2008) 503–532.
[24] P. Grisvard, Elliptic Problems in Nonsmooth Domains, Society for Industrial and Applied Mathematics, 2011.
[25] T.-P. Fries, Overview and comparison of different variants of the XFEM, Proc. Appl. Math. Mech. 14 (2014) 27–30.
[26] N. Newmark, A method of computation for structural dynamics, in: Proceedings of the ASCE, J. Eng. Mech. Div. 85 (1959) 67–94.
[27] T. Elguedj, A. Gravouil, H. Maigre, An explicit dynamics extended finite element method. Part 1: mass lumping for arbitrary enrichment functions, Comput. Methods Appl. Mech. Eng. 198 (2009) 2297–2317.
[28] J.R. Rice, A path independent integral and the approximate analysis of strain concentration by notches and cracks, J. Appl. Mech. 35 (1968) 379–386.
[29] L. Wen, L. Wang, R. Tian, Accurate computation on dynamic sifs using improved xfem, Chin. J. Theoret. Appl. Mech. 50 (2018) 599–610.
[30] E. Bouchbinder, T. Goldman, J. Fineberg, The dynamics of rapid fracture: instabilities, nonlinearities and length scales, Rep. Prog. Phys. 77 (2014) 046501.
[31] M. Rahman, T. Michelitsch, A note on the formula for the Rayleigh wave speed, Wave Motion 43 (2006) 272–276.
[32] M. Imachi, S. Tanaka, M. Ozdemir, T.Q. Bui, E. Oterkus, Dynamic crack arrest analysis by ordinary state-based peridynamics, Int. J. Fract. 221 (2020).
[33] W. Tian, J. Huang, Y. Jiang, R. Chen, A parallel scalable domain decomposition preconditioner for elastic crack simulation using XFEM, Int. J. Numer. Methods Eng. 123 (15) (2022) 3393–3417.
[34] H. Waisman, L. Berger-Vergiat, An adaptive domain decomposition preconditioner for crack propagation problems modeled by xfem, Int. J. Multiscale Comput. Eng. 11 (6) (2013) 633–654.
[35] X. Chen, X.-C. Cai, Effective two-level domain decomposition preconditioners for elastic crack problems modeled by extended finite element method, Commun. Comput. Phys. 28 (4) (2020) 1561–1584.
[36] Y. Saad, Iterative Methods for Sparse Linear Systems, Society for Industrial and Applied Mathematics, 2003.
[37] X.-C. Cai, Y. Saad, Overlapping domain decomposition algorithms for general sparse matrices, Numer. Linear Algebra Appl. 3 (3) (1996) 221–237.
[38] X.-C. Cai, M. Sarkis, A restricted additive Schwarz preconditioner for general sparse linear systems, SIAM J. Sci. Comput. 21 (2) (1999) 792–797.
[39] L.B. Freund, Dynamic Fracture Mechanics, Cambridge University Press, Cambridge, 1990.
[40] H. Hilber, T. Hughes, Collocation, dissipation and “overshoot” for time integration schemes in structural dynamics, Earthq. Eng. Struct. Dyn. 6 (1978) 99–118.
[41] G. Hilbert, T. Hughes, An error analysis of truncated starting conditions in step-by-step time integration: consequences for structural dynamics, Earthq. Eng. Struct. Dyn. 15 (1987) 901–910.